frontiers

Supplementary Material

Numerical modelling shows increased fracturing due to melt-undercutting prior to major calving at Bowdoin Glacier

E. C. H. van Dongen, J. A. Åström, G. Jouvet, J. Todd, D. I. Benn and M. Funk

This supplement includes additional information regarding the Helsinki Discrete Element Model (HiDEM) and sensitivity experiments.

1 HIDEM

1.1 Overview

The HiDEM version we use here, models ice as a brittle-elastic material. That is, irreversible material strain like creep, plasticity and viscosity are not included in the model. Apart from elastic deformation and instantaneous fracture, the model also includes basal friction. Additional external forces that act on DEM-particles are: gravity, buoyancy, and drag. When particles collide and beams oscillate there is dissipation of kinetic energy through a force proportional to relative velocity of DEM-particles or beam end-points.

The hexagonal close packed (hcp) lattice in which particles are initially arranged is a close-packing configuration for equal-sized spheres with solid-volume fraction of 0.74. Every sphere in the bulk of the material has 12 neighbours. Since the beams have a stiffness of the same order of magnitude for all deformation modes, the particles closely approximate a homogeneous medium. The mass of the DEM-particles is set such that the density of the material-model is ρ= 930 kg m^{-3}. The stiffness of the beams connecting neighbours, can be related to Young's modulus E of the material (Åström et al., 2013) and are set such that $E = 1$ GPa (a common value for polycrystalline glacier ice, Vaughan, 1995). Poisson's ratio in HiDEM has a complex dependence on model parameters and implementation but is ∼0.2 (Riikilä et al., 2015).

1.2 Equation of motion

The ice dynamics are computed using a discrete version of Newton's equation of motion and inelastic potentials for the interactions of individual particles and beams:

$$\boldsymbol{M}\ddot{\boldsymbol{r}}_{\boldsymbol{i}} + \boldsymbol{C}\dot{\boldsymbol{r}}_{\boldsymbol{i}} + \sum_j \boldsymbol{C'}(\dot{\boldsymbol{r}}_{\boldsymbol{i}} - \dot{\boldsymbol{r}}_{\boldsymbol{j}}) + \sum_j \boldsymbol{K_p}(\boldsymbol{r_i} - \boldsymbol{r_j}) + \sum_j \boldsymbol{K_b}(\boldsymbol{r_i} - \boldsymbol{r_j}) = F_i, \tag{S1}$$

where $\boldsymbol{M}$ contains the masses and moments of inertia of the particles, $\ddot{\boldsymbol{r}}_{\boldsymbol{i}}, \dot{\boldsymbol{r}}_{\boldsymbol{i}}$ are the acceleration and velocity of particle i, including rotations. The indices for all particles that are connected to particle i are denoted with j.

Particles are damped by a viscous drag, denoted by the damping matrix $\boldsymbol{C}$. The damping coefficients depend on the particles position, since particles are either in contact with the bedrock, water or air. The damping coefficients do not change in a discrete manner but linearly over a zone of 1 particle size at the water line and 1.5 particle size at the bedrock for stability reasons. The bedrock damping coefficient may vary in space, to model the variation in slipperiness of the bed. The water drag force is estimated by the drag force of a square-metre objects in water (10^3 kg s^{-1}, Åström et al., 2013).

Collisions between particles are inelastic. The damping force for collisions, $\boldsymbol{C'(\dot{r}_i - \dot{r}_j)}$, is velocity-dependent and allows dissipation of energy. Dissipation C' can be estimated via an analog to a harmonic oscillator. On a microsopic level, DEM-particles and beams form a set of coupled harmonic oscillators. If the oscillators are overdamped, sound waves cannot propagate properly in the material, which would not be a good model for ice. If the oscillators are very much underdamped, the particles would bounce around during calving, which is clearly not realistic for ice. Therefore we use values for C' that correspond to slightly underdamped values (Åström et al., 2013).

The interactions between particles that are in contact, regardless of having a beam connecting them or not, are modelled as a Hertz contact problem (Hertz, 1882). The elastic, radial repulsive interaction is denoted by $\boldsymbol{K_p(r_i - r_j)}$. Interactions between particles that are connected by a beam, are contained in the stiffness matrix $\boldsymbol{K_b(r_i - r_j)}$. Their interaction is modelled as a Euler-Bernoulli beam (Åström et al., 2013), which describes the deflection of a beam under an applied load in a linear elastic manner and holds for small strains. Without the Euler-Bernoulli beams, the particles would move as granular flow.

Finally, the sum of other forces working on particle i is denoted by F_i. For particles above sea level this includes gravity $F_g = \rho_i g V$ and for particles below sea level a buoyancy force $F_b = (\rho_i - \rho_w) g V$ where ρ_i, ρ_w are the ice and water density, g the gravitational acceleration and V the volume of the particle. The buoyancy force is applied for all submerged ice particles, because it is not trivial to define a surface (for example the calving front) in a Discrete Element Model. However, a buoyancy force for all submerged particles is equivalent to application of the water pressure at the calving front and floating ice base, as usually done in glacier models (e.g., Todd et al., 2018). The equivalence can be explained by a consideration of the involved pressures. The pressure within the ice increases with ice depth, d, as $\rho_i g d$. The pressure of the water increases with water depth, h, $\rho_w g h$. The pressure within the ice below sea surface can then be written as: $\rho_i g l + \rho_i g (d - l)$, where, l is the ice-cliff height above sea surface, which means $h = d - l$. We then get for the pressure $\rho_i g l + \rho_i g h - \rho_w g h + \rho_w g h$, which can be written as $\rho_i g l + (\rho_i - \rho_w) g h + \rho_w g h$. The first term is the overburden pressure for the ice above sea level, the second term is the deviatoric term from the difference between ice and water pressure, and the last term is the pure hydrostatic pressure. Since we can assume that both water and ice are incompressible, and if we further assume that water penetrates all cracks below sea level, we can neglect the last hydrostatic term in the computations since it does not induce any dynamics. Therefore, the dynamics induced by buoyancy can be modelled by the previously introduced forces F_g and F_b.

1.3 Time integration

The differential equation for motion (Eq. S1) is rewritten as a difference equation and integrated forward in time using explicit time integration. A crude estimate of the desired time step for this type of calculations can be derived from an analog to the resonance frequency of a harmonic oscillator $\sqrt{Ed/m}$, where E is the stiffness of the beams, d is diameter of the particles and m the particle mass. Hence for spheres with a radius of 1 m and $E \approx 10^9$ N m^{-2}, the resonance frequency is on the order of 10^3 s^{-1}. Multiplied by the particle size this gives rise to velocities on the order of 10^3 m s^{-1}, which should be resolved in at least 10 time steps. Therefore, for particles of 1 m radius, a minimum time step of 10^{-4} s is required.

1.4 Fracture criterion

Beams break if the strain on the beam exceeds a user-defined threshold ε_c, either by tension or bending:

$$\varepsilon_\ell + 0.05|\theta_i - \theta_j| \geq \varepsilon_c \tag{S2}$$

where ε_ℓ denotes axial strain and $\theta_i - \theta_j$ rotations at the ends of the beam. We set $\varepsilon_c = 0.0003$. Since the model is brittle-elastic and tensile fracturing dominates, fracture-strain is easily translated into to the more commonly used fracture-stress by multiplying with Young's modulus. We then have a fracture stress of 0.3 MPa, which is within the range of observed critical stress (Schulson, 1999).

2 SENSITIVITY EXPERIMENTS

2.1 Particle size

Unlike mesh size for continuum models, the particle size for DEM has a direct physical meaning: it matters whether the glacier is built up of particles of similar size as sand grains or bricks. In an idealized world with extremely fast computers, one could model a glacier by representing each ice crystal as a particle. Even when running HiDEM on a supercomputer for a small part of a glacier, the particle size needs to compromise accuracy and efficiency. We test which particle size, defined as particle diameter, best reproduces fracturing on Bowdoin Glacier. The largest applied particle size is 10 m, as chosen in Vallot et al. (2018) for Kronebreen. However, although terminus thickness of Bowdoin Glacier and Kronebreen are similar, this particle size does not yield large enough strain to cause fracturing on Bowdoin Glacier (results not shown). Therefore, particle size was reduced in several steps from 4 to 1.75 m.

The simulation consist of two phases. First initial glacier dynamics are simulated without fracturing, such that the glacier reaches a state which is reasonably close to a stress equilibrium. Kinetic energy is defined as

$$\Sigma_i \frac{1}{2} m_i v_i^2 \tag{S3}$$

where m_i is particle mass and v_i velocity, summed over all particles i. Figure S1 shows for all tested particle sizes how the kinetic energy of the glacier reduces during 15 s of simulation.

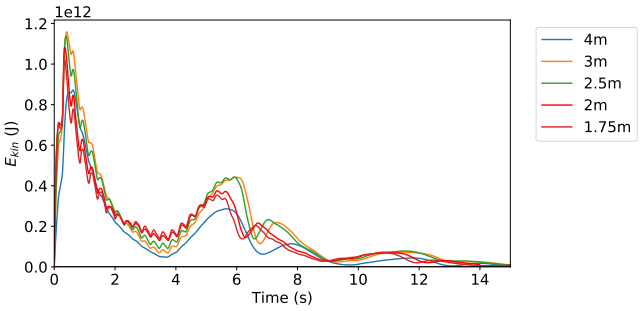

Figure S1. Time evolution of kinetic energy for various particle sizes.

After 10 s, the kinetic energy is reduced by more than an order of magnitude and fracturing is allowed. The resulting surface crevasse pattern after 15 s of simulation time is shown in Figure S2. The HiDEM results are sensitive to DEM-particle size. In particular, the glacier becomes more fragile, and a larger portion of bonds break when particle size decreases and particle number grows. The density of broken bonds in the model domain, which reflects the abundance of fractures, increases with decreasing particle size from 0.7% for 4 m particles to 2.3% for 1.75 m particles (Fig. S2). A rather unexpected effect of this is that larger particle size reproduces the velocity field better than smaller ones, as the velocity field gets increasingly scrambled by fracturing. For 4-2.5 m particles, the surface velocity in the final second of the

simulation reproduces the observed velocity gradient well (Fig. S3a-c). The velocity gradient is less clearly for smaller particles because fracturing dominates the modelled velocity (Fig. S3d and e).

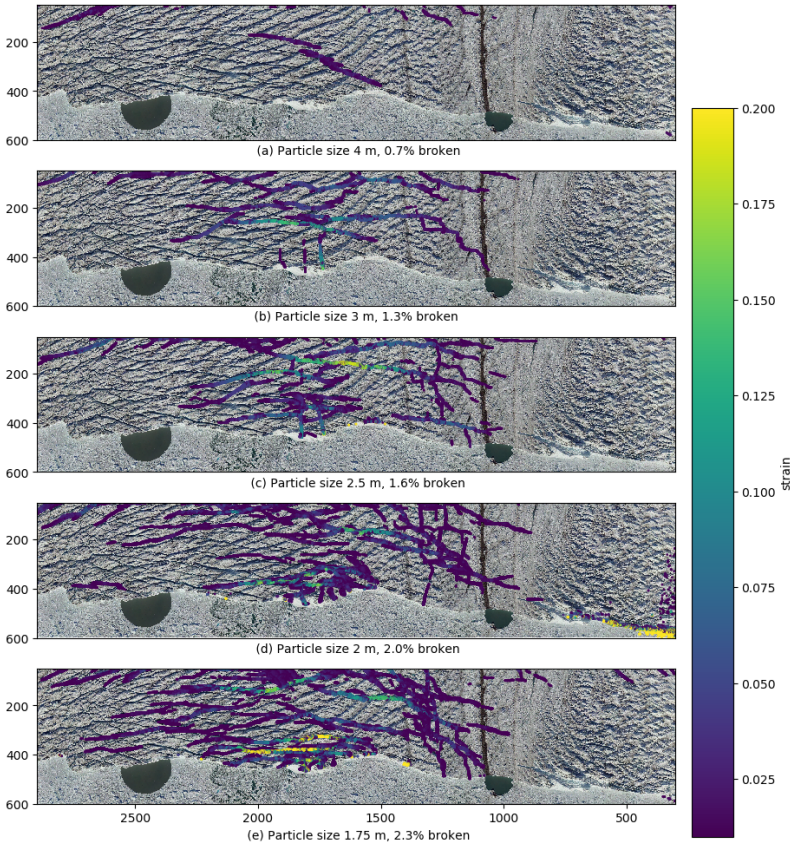

Figure S2. All bonds above sea level with fracture strain over 0.01 for several particle sizes after 15 s. Colors show the strain for each bond, which is a measure of crevasse width and subplot labels give the percentage of broken bonds for the entire model domain.

2.2 Smoothed surface

The observed glacier geometry is very detailed with surface topographic depressions included. In the UAV-derived surface elevation, these depressions extend down to about 5m, which is small compared to the thickness of the glacier (more than 250 m, Fig. 2b). These features are nevertheless sufficient for fractures formed in the simulations to often appear exactly along these grooves, especially for small particles (Fig. S2e).

The 1 m resolution DSM was filtered by a two dimensional median filter with a 51×51 kernel to study the impact of the detailed initial geometry. To limit the required computational resources, this was done for particles of 2.5 m only. The modelled surface fractures are very similar (Fig. S4), although the smooth surface simulation shows more fractures aligned with the direction of flow.

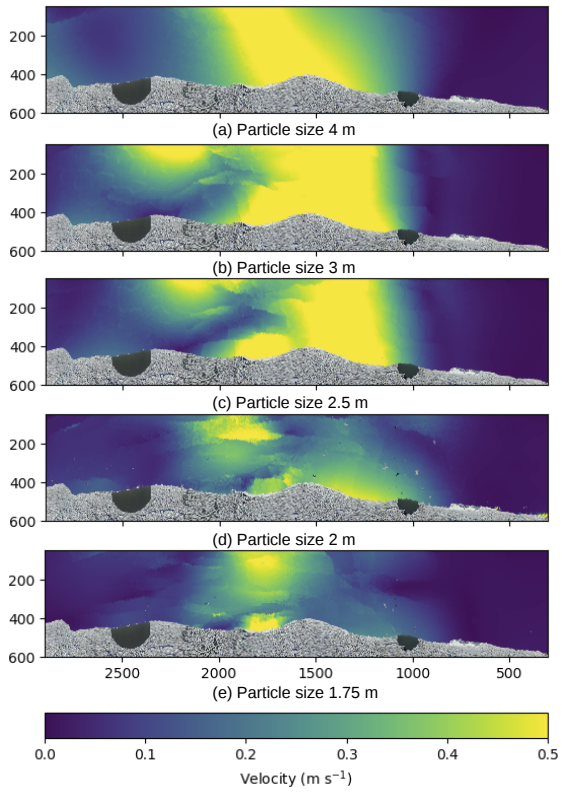

Figure S3. Modelled velocity from 14 to 15 s for varying particle size.

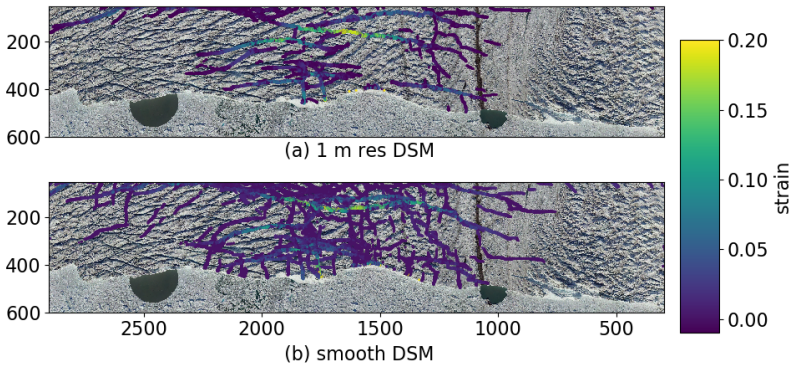

Figure S4. All bonds above sea level with fracture strain over 0.01 are shown for 2.5 m particles after 15 s for the control set-up (a) and a smoothed surface (b).

Table S1. Numerical values of the constants used in the numerical experiments.

Parameter	Symbol	Value	Unit
Ice density	ρ	930	kg m^{-3}
Water density	ρ_w	1030	kg m^{-3}
Gravitational acceleration	g	9.81	m s^{-2}
Strain threshold	ε_c	0.0003	
Timestep		10^{-4}	s
Fracture after time		10	s
Friction scale		10^{-5}	

REFERENCES

Åström, J. A., Riikilä, T. I., Tallinen, T., Zwinger, T., Benn, D., Moore, J. C., et al. (2013). A particle based simulation model for glacier dynamics. *Cryosphere* 7, 1591–1602. doi:10.5194/tc-7-1591-2013

Hertz, H. (1882). Ueber die berührung fester elastischer körper. *J. reine angew. Math.* 92, 156–173

Riikilä, T., Tallinen, T., Åström, J., and Timonen, J. (2015). A discrete-element model for viscoelastic deformation and fracture of glacial ice. *Comput. Phys. Commun.* 195, 14 – 22. doi:https://doi.org/10.1016/j.cpc.2015.04.009

Schulson, E. M. (1999). The structure and mechanical behavior of ice. *Jom* 51, 21–27

Todd, J., Christoffersen, P., Zwinger, T., Råback, P., Chauché, N., Benn, D., et al. (2018). A Full-Stokes 3-d Calving Model Applied to a Large Greenlandic Glacier. *J. Geophys. Res.: Earth* 123, 410–432. doi:10.1002/2017JF004349

Vallot, D., Åström, J., Zwinger, T., Pettersson, R., Everett, A., Benn, D. I., et al. (2018). Effects of undercutting and sliding on calving: a global approach applied to Kronebreen, Svalbard. *Cryosphere* 12, 609–625. doi:10.5194/tc-12-609-2018

Vaughan, D. G. (1995). Tidal flexure at ice shelf margins. *J. Geophys. Res.: Solid Earth* 100, 6213–6224